Stereospecific Ziegler−Natta Model Catalysts Produced by Electron Beam-Induced Deposition of $TiCl_4$: Deposition Kinetics, Film Structure, and Surface Structure

Seong Han Kim[†] **and Gabor A. Somorjai***

Department of Chemistry, University of California at Berkeley and Materials Science Division, Lawrence Berkeley National Laboratory, Berkeley, California 94720

Received: August 20, 2000; In Final Form: November 19, 2001

A multilayer film of $TiCl_x$, model Ziegler−Natta catalyst for stereospecific polymerization, was produced by electron beam-induced deposition of $TiCl_4$ on an Au substrate at 100 K. The deposition of solid-phase $TiCl_x$ took place by dissociation of $TiCl_4$ adsorbed at the substrate surface by electrons—both primary and secondary. The deposition kinetics, surface composition, and structure were studied with X-ray photoelectron spectroscopy and temperature-programmed desorption. Its polymerization stereochemistry was studied by analyzing the polypropylene products with infrared spectroscopy and atomic force microscopy. The deposited film was stable at temperatures lower than 450 K and had a high concentration of chemisorbed $TiCl_4$ species. The film surface was composed of mostly a nonbasal plane (defective) structure. When activated by reactions with $Al(C_2H_5)_3$, the $TiCl_x$ film selectively produced isotactic polypropylene. The absence of atactic polypropylene was due to the lack of $TiCl_x$ sites with the basal plane structure, caused by the deposition method involving high-energy electrons and low substrate temperature.

I. Introduction

Production of stereospecific Ziegler−Natta polymerization catalysts and characterization of their surface composition and structure can provide molecular-level understanding of the stereochemistry involved in production of isotactic polypropylene. Industrial catalysts, $TiCl_4$ supported on high-surface-area $MgCl_2$, use one or a combination of Lewis bases to obtain polypropylene with high isotacticity.[1,2] Studies of these catalysts with conventional characterization techniques could not provide an unambiguous description of the nature of active sites on the catalyst surface due to the complexity of the surface composition and structure of the high-surface-area catalyst system. Surface-sensitive characterization techniques, using electrons and ions, could not be applied directly to the industrial catalysts due to surface charging problems of the nonconducting materials.[3,4]

To overcome the charging problems and utilize modern surface science techniques, we have synthesized a series of titanium chloride thin films on a gold substrate.[5−14] These films could be activated for Ziegler−Natta polymerization producing polyethylene and polypropylene. Their surface composition and structure could be characterized by X-ray photoelectron spectroscopy (XPS), Auger electron spectroscopy (AES), ion scattering spectroscopy (ISS), low-energy electron diffraction (LEED), and temperature-programmed desorption (TPD). These studies allowed direct correlation between the surface characterization data of the model catalysts and the stereochemical analysis data of the polypropylene products.[14]

Among model catalysts we studied, a $TiCl_x$ multilayer film fabricated by electron beam-induced deposition of $TiCl_4$ on Au produced highly isotactic polypropylene in the absence of any Lewis base.[14] This paper describes in detail the fabrication and characterization of the $TiCl_x$ multilayer film deposited by electron irradiation and its stereospecific polymerization of propylene. The $TiCl_4$ molecules were adsorbed on Au at 100 K and then dissociated by interactions with electrons. The low substrate temperature and high flux irradiation of electrons allowed the accumulation of chemisorbed $TiCl_4$ species to a high concentration and the exposure of nonbasal (defective) structures at the film surface, which were responsible for the stereospecific polymerization of propylene.

II. Experimental Section

The experimental apparatus, an UHV chamber combined with an internal high-pressure reaction cell (HP), has been described in detail elsewhere.[10] Briefly, the UHV chamber was equipped with a sputter ion gun for surface cleaning, an X-ray source and a double-pass cylindrical mirror analyzer with a coaxial electron gun for XPS and AES, a quadrupole mass spectrometer (QMS) for residual gas analysis and TPD, three leak valves for gas exposure, and an electron flood gun (electron beam diameter $\approx$ 2 cm^2) for electron irradiation onto the sample. A commercially available UHV sample manipulator provided three-dimensional translation and 360° rotation of the sample.

A polycrystalline Au foil (1.2 cm^2) was spot-welded onto Au wires, which were spot-welded onto the Ta posts that were attached to liquid-N_2 cooled electrodes. This assembly had capability to heat the Au foil resistively to >900 K and cool to 100 K. The sample temperature was measured with a type-K thermocouple attached to the back of the foil. The Au foil was cleaned with Ar ion sputtering followed by annealing at 900 K. $TiCl_4$, mesitylene (1,3,5-trimethylbenzene), and $Al(C_2H_5)_3$ were purified by several freeze−pump−thaw cycles. Polymer-grade propylene was passed through an oxygen/water trap before use.

Gas admittance into the UHV chamber was controlled with three leak valves. One leak valve used for $TiCl_4$ exposure was equipped with a 1/8-in. stainless steel tube that extended to the

* Corresponding author. E-mail: somorjai@socrates.berkeley.edu.
[†] Current address: Department of Chemical Engineering, The Pennsylvania State University, University Park, PA 16802.

10.1021/jp013239q CCC: $22.00
Published on Web 01/22/2002

front of the sample. This $TiCl_4$ doser had a pressure enhancement of ~3 compared to the others.[10] Nominal pressures reported in this paper were readouts of a Bayard-Alpert ion gauge, located about 20 cm away from the sample, without correction for ionization sensitivity and dosing geometry. The electron flux was calculated from the measured beam current divided by the sample area. Integration of this electron flux over irradiation time gave total electron dose per unit area.

In TPD of the $TiCl_x$ film, the deposited film was resistively heated to 900 K at a rate of 4 K/s. In TPD of mesitylene on $TiCl_x$, the film at 100 K was exposed to mesitylene (exposure unit: $1\ L = 1 \times 10^{-6}$ Torr s) and then resistively heated at a rate of 4 K/s. Desorbing species from the film surface were detected with QMS. The QMS ionizer, facing the sample, was covered with a shroud with a small aperture, to reduce the effect of background desorption. In XPS analysis, the Al Kα radiation (1486.6 eV) was used and the angle between the surface normal and the CMA axis was 35°. The Au $4f_{7/2}$ peak was taken as a reference for the energy scale. The XPS spectra of Ti reported in the following section have been background subtracted and deconvoluted into a series of synthetic peaks (67% Gaussian and 33% Lorentzian; fwhm = 2.3 eV) that represent the photoelectron emission from different oxidation states.[15] The XPS of the $TiCl_x$ films was measured at 300 K. The fitting parameters of the synthetic peaks were determined from the Ti 2p spectrum of $TiCl_4$ physisorbed at 100 K.[10] During AES measurements, the beam current of the primary electrons was kept lower than 1 μA.

Propylene polymerization was performed in the HP cell. The catalyst was activated by exposure to ~1 Torr of the $Al(C_2H_5)_3$ vapor (cocatalyst) at a sample temperature of 300 K. After excess $AlEt_3$ was pumped out, propylene was introduced in the HP cell to ~900 Torr and the sample temperature was increased to 340 K. A few hours later, the HP cell was evacuated and the polymer film covering the catalyst surface was analyzed with XPS and TPD in UHV.

The polypropylene films produced with model catalysts were further analyzed with FTIR and AFM. FTIR spectra of the as-grown polymer films on the substrate were measured in an attenuated total reflection (ATR) mode. Contact-mode AFM images were taken for as-grown polymers and solvent-extracted polymers. The atactic and isotactic fractions of the produced films were sequentially extracted with *n*-hexane and *n*-octane.[16−18] Each extracted fraction was cast on a slide glass, dried at 25 °C, and characterized with AFM. The force constant of the cantilever used was 0.05 N/m. Topographic images were taken at a normal load of 0.6 nN and 2.0 nN.

III. Results

III-1. Stereospecific Polymerization of Propylene on $TiCl_x$ Model Catalyst. Electron beam irradiation on an Au substrate during the exposure to $TiCl_4$ produced $TiCl_x$ multilayer films that were active for Ziegler−Natta polymerization. The $TiCl_x$ films were activated by exposure to $Al(C_2H_5)_3$ vapor. The activated films were able to polymerize ethylene and propylene in the absence of excess cocatalyst.[11,12,14] In contrast to the high-surface-area catalysts that need a Lewis base such as ethyl benzoate to increase isotactic polypropylene yields, the $TiCl_x$ model catalyst selectively produced isotactic polypropylene without using any Lewis base.[14]

Figure 1 summarizes XPS, ATR-IR, and solvent fractionation data of polypropylene films produced with the $TiCl_x$ model catalysts. The polymer thickness was typically hundreds of nanometers depending on polymerization conditions.[12] With

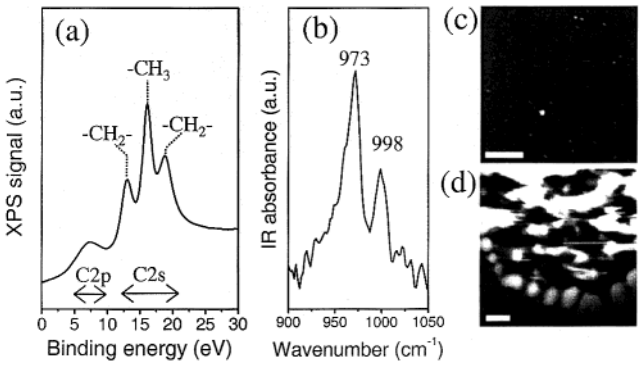

Figure 1. (a) XPS and (b) ATR-IR data of a polypropylene film produced with a $TiCl_x$/Au model catalyst; and AFM images polypropylene extracted by (c) hexane and (c) octane. In (b), the peak at 998 cm^{-1} is associated with isotactic helix vibration and the peak at 973 cm^{-1} is an internal reference for C−C vibration (see text for details). In (c) and (d), the scale bar indicates 5 μm; and the dark gray background is a glass substrate and the white regions are polymer particles. Catalyst: a $TiCl_x$ multilayer film. Polymerization time: 4−5 h. Other polymerization conditions are described in Experimental Section.

XPS, no signals for the Ti, Cl, and Au components were detected, only carbon at 285 eV. The high-resolution valence-band XPS (Figure 1a) showed three-peak features in the C2s region, a characteristic spectrum of polypropylene.[19,20] Two peaks at ~14 and 18.3 eV are assigned to the C2s electrons in the $-CH_2-$ backbone with antibonding and bonding interactions with neighboring C2s electrons, respectively. The peak at 16 eV corresponds to the C2s electrons in the $-CH_3$ group.

The ATR-IR analysis of the as-grown polypropylene film (Figure 1b) showed an intense peak at 998 cm^{-1} associated with the isotactic helix vibration.[18] The solvent fractionation analysis, combined with AFM, clearly revealed the high isotacticity of the polypropylene film produced with the $TiCl_x$ model catalyst: *no atactic polypropylene was extracted with hexane (Figure 1c) while a significant amount of isotactic polypropylene was extracted with octane (Figure 1d)*. A small particle shown in Figure 1c was believed to be isotactic PP on the basis of its hardness. Atactic polypropylene would be pushed out from the scan region at the load used in this experiment (2 nN).[14] From these results, it could be concluded that the $TiCl_x$ catalyst produces exclusively isotactic polypropylene.

III-2. Fabrication of $TiCl_x$ Model Catalysts by Electron Irradiation. $TiCl_4$ did not react with the Au substrate and desorbed intact at ~250 K from the first monolayer and ~170 K from multilayers. When an electron beam irradiated the $TiCl_4$ layers adsorbed on the substrate at 100 K, a solid phase of $TiCl_x$ was formed which was stable in the typical polymerization temperature range (300−370 K). Electron beam irradiation could be done during or after the $TiCl_4$ adsorption at 100 K. In this paper, we focus on the simultaneous irradiation by the electron beam during the $TiCl_4$ adsorption. The post-adsorption irradiation produced $TiCl_x$ films that had thermal evaporation and titanium oxidation state distributions similar to the ones produced by simultaneous irradiation.

The effects of electron flux and energy on the $TiCl_x$ film deposition yields were studied in a low electron flux region ($<1 \times 10^{14}$ electrons $cm^{-2}\ s^{-1}$) to understand the mechanisms of depositing $TiCl_x$ on the Au substrate. Figure 2a shows the electron flux dependence of the $TiCl_x$ film deposition at constant electron energy (500 eV). The $TiCl_4$ pressure was 9×10^{-8} Torr and the deposition time was 8 min. The amount of $TiCl_x$ deposits was presented by the area of the $TiCl_3^+$ TPD peak.

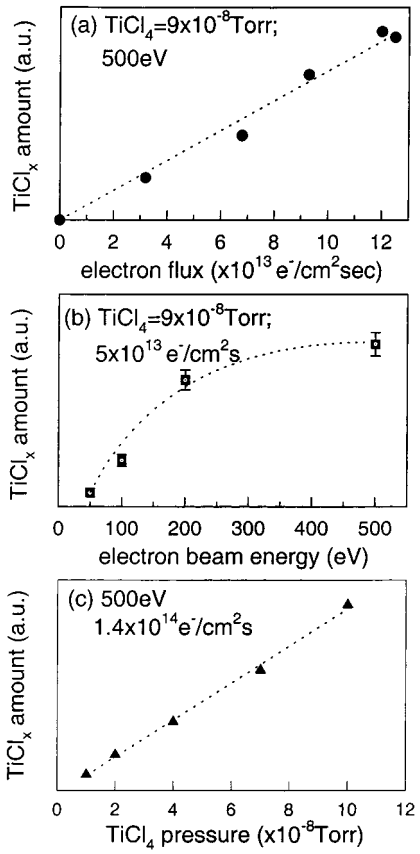

Figure 2. Dependence of the $TiCl_x$ deposited amount on (a) electron flux at a constant electron energy, (b) electron energy at a constant flux, and (c) $TiCl_4$ pressure. The amount of $TiCl_x$ deposits was obtained by integrating the $TiCl_3^+$ ion profile in TPD. The deposition time was 8 min.

The data showed that the deposition yield increased in proportion to the electron flux, indicating first-order kinetics with respect to electron flux.

Figure 2b shows the electron energy dependence of the $TiCl_x$ film deposition at a constant electron flux (5×10^{13} electrons cm^{-2} s^{-1}). The deposition yield increased nonlinearly with increasing the electron energy (E) from 50 to 500 eV. The data were fitted with Vaugan's formula, a universal formula describing secondary electron yield, $\delta(E)$, as a function of electron impact energy (E):[21,22]

$$\delta(E)/\delta_{max} = (\nu e^{1-\nu})^k$$

where δ_{max} = the maximum yield of the secondary electrons, E_{max} = the electron energy where the secondary electron yield is the highest, $\nu = (E - 12.5\ eV)/(E_{max} - 12.5\ eV)$, and $k = 0.62$ for $E < E_{max}$ and 0.25 for $E > E_{max}$. The fit curve shown in Figure 2b was obtained with assumptions of $E_{max} = 500$ eV and a first-order kinetics for reactions of $TiCl_4$ with secondary electrons. The good fit indicated the involvement of secondary electrons in the $TiCl_x$ deposition (see Section IV-1).

The $TiCl_4$ pressure dependence of the film deposition is shown in Figure 2c. The plot of TPD area versus $TiCl_4$ pressure showed a first-order dependence of the $TiCl_x$ deposition to $TiCl_4$ pressure. At 100 K, all the $TiCl_4$ molecules impinging on the surface were adsorbed into a condensed layer, which then converted to $TiCl_x$ deposits by electron beam irradiation.

When the film surface areas were compared by measuring the saturation exposure of a probe molecule (mesitylene) to complete a monolayer, it was found that the surface areas of the $TiCl_x$ films were significantly larger than that of the Au substrate area (data not shown). This result also supported the conversion of condensed $TiCl_4$ molecules into $TiCl_x$ deposits. During the film deposition, $TiCl_4$ molecules colliding with the surface held at 100 K would adsorb at their initial collision sites. Because the gas-phase molecules impinged randomly on the surface, the condensed film had a rougher surface as the film grew thicker and its surface area increased in proportion to the square root of the film thickness.[23,24]

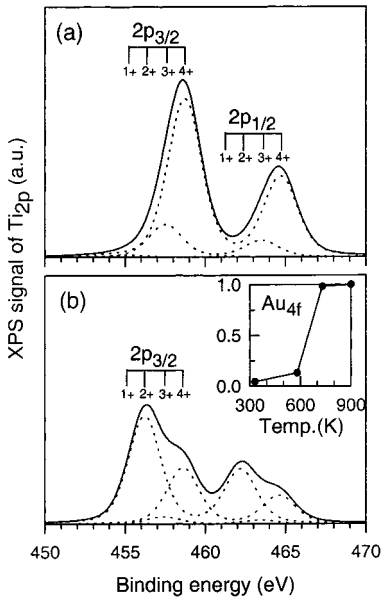

Figure 3. Ti2p XPS of the $TiCl_x$ film (a) before and (b) annealing at 580 K. The peak positions for different Ti oxidation states were indicated as 1+, 2+, and 3+, and 4+. The inset to (b) shows the XPS intensity of the Au $4f_{7/2}$ peak at 94 eV as a function of annealing temperature. Deposition conditions: $P(TiCl_4) = 1 \times 10^{-7}$ Torr, electron energy = 500 eV, electron flux = 1.5×10^{14} electrons cm^{-2} s^{-1}, deposition time = 13 min.

TABLE 1: Ti Oxidation State Distribution (%) in the $TiCl_x$ Film Deposited by 500 eV Electron Irradiation (XPS measurement: 300 K)

	Ti oxidation state				
treatment	4+	3+	2+	1+	0
as-dosed[a]	82	17	0	1	0
annealed[b]	32	4	63	1	0

[a] Deposition condition described in Figure 3. [b] Annealing temperature = 580 K.

III-3. Characterization of $TiCl_x$ Model Catalysts Deposited at 100 K. *3a. Ti Oxidation States in $TiCl_x$ Multilayer Film.* The XPS data of the Ti_{2p} region are reported in Figure 3. For the as-deposited multilayer film, Ti^{4+} ions were ~82% and Ti^{3+} ions were ~17% (Table 1). This oxidation state distribution did not vary significantly with increasing deposition time. Since the solid phase of pure $TiCl_4$ is not stable at 300 K where XPS was taken,[25,26] the Ti^{4+} signal must come from the chemisorbed $TiCl_4$ species. There was no oxygen peak detected, indicating the absence of TiO_2. The large Ti^{4+} signal of the deposited film suggested that the film surface is almost completely covered with chemisorbed $TiCl_4$ molecules. Upon annealing to 580 K (Figure 3b), the Ti^{4+} peak decreased to 32% of the total Ti intensity and the Ti^{2+} peak increased to 63%.

The film thickness was estimated from the attenuation of the Au substrate signal (inset to Figure 3b).[27] Though the CMA provided an angle-averaged intensity over its acceptance solid angle, we made a crude assumption that the measured intensity

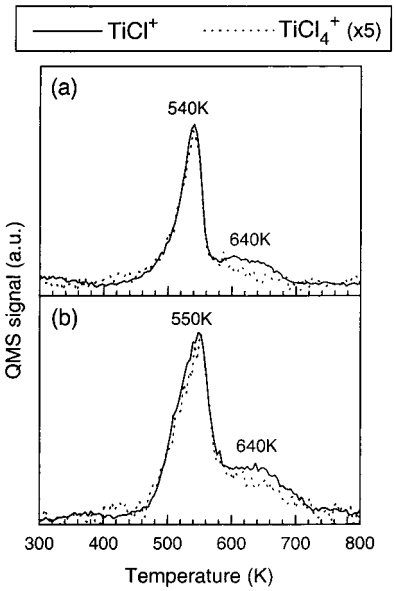

Figure 4. TPD of $TiCl_x$ film deposited at 100 K for (a) 10 min and (c) 40 min. $P(TiCl_4)$ was 1×10^{-7} Torr and the electron energy and flux was 500 eV and 1.6×10^{14} electrons cm^{-2} s^{-1}.

could be treated as an angle-resolved intensity at the CM*A* axis (35° from the surface normal). Considering a mean free path of Au_{4f} photoelectrons of 20 Å,[28] the film thickness was estimated at ∼5.3 nm for the film deposited at $P(TiCl_4) = 1 \times 10^{-7}$ Torr and electron flux $= 1.5 \times 10^{14}$ electrons cm^{-2} s^{-1} for 13 min. Its thickness decreased to ∼3.5 nm upon annealing at 580 K. After annealing at 720 K, the Au signal intensity was almost completely recovered, suggesting that most of the $TiCl_x$ deposits were desorbed.

3b. Thermal Evaporation of $TiCl_x$ Film. Figure 4 presents $TiCl^+$ and $TiCl_4^+$ ion profiles recorded during the TPD of $TiCl_x$ films deposited for 10 and 40 min. To make comparison easier, the $TiCl_4^+$ ion profile was multiplied by a factor of 5, the fragmentation ratio of the gas-phase $TiCl_4$ in our QMS. (The $TiCl_2^+$ and $TiCl_3^+$ ion signals were also recorded simultaneously, but they are not shown here for simplicity because they implied the same conclusion.) The TPD profile of the $TiCl_x$ multilayer film showed two peaks regardless of deposition time: a large desorption peak at ∼540 K and a small peak at ∼640 K. The only observable change in TPD was an increase in signal intensity as a thicker film was formed at a longer deposition time. The peak at ∼540 K had the $TiCl_y^+$($y = 1$, 2, 3) ion profiles following the $TiCl_4^+$ ion profile, indicating fragmentation of $TiCl_4$(g). Above 580 K, the $TiCl_y^+$($y = 1$, 2, 3) ion profiles did nor follow the $TiCl_4^+$ ion profile and were larger than the fragmentation ratio of $TiCl_4$ in QMS.

On the basis of the XPS results, the 540 K peak was tentatively assigned to desorption of $TiCl_4$(g) from chemisorbed $TiCl_4$ species and/or decomposition of the $TiCl_3$ phases. The desorption of chemisorbed $TiCl_4$ species was quite obvious from the large decrease in the Ti^{4+} intensity upon annealing to 580 K (Table 1). The reduction of film thickness by 1.5−2 nm (inset to Figure 3b) implied that some portion of the film decomposes producing $TiCl_4$(g) upon annealing to 580 K. The desorption of chemisorbed species alone could not cause such a large reduction in film thickness. The decrease of the Ti^{3+} intensity (Table 1) suggested the decomposition of $TiCl_3$ phase. With a Redhead model for first-order desorption process[29] and an assumption of the preexponential factor $\nu = 10^{13}$ s^{-1}, the heat of desorption for the 540 K peak was estimated at ∼34 kcal/mol. This value was within the range measured experimentally for the heat of $TiCl_4$ vaporization from disproportionation of $TiCl_3$ solid phases (31−40 kcal/mol).[30−32]

The desorption profiles at $T > 580$ K were assigned to decomposition of chlorine-deficient phases producing $TiCl_3$(g), $TiCl_2$(g), and/or Ti_2Cl_6(g), rather than $TiCl_4$(g).[26,30] The XPS results showed that a large fraction of titanium was in the 2+ oxidation state. It should be noted that the $TiCl_y^+$($y = 1$, 2, 3, and 4) intensities at $T < 580$ K was more than twice those at $T > 580$ K while the film thickness decreased by only a third upon heating to 580 K (inset to Figure 3). This implied low desorption yields of $TiCl_3$(g), $TiCl_2$(g), and Ti_2Cl_6(g) from the chlorine-deficient phase, which was consistent with that fact that the formation of these molecules is thermodynamically less favorable compared to the formation of $TiCl_4$ molecules.[26,30]

As the substrate temperature increased further, the desorption of $TiCl_y$ ($y > 1$) species increased the ratio of titanium to chlorine in the film remaining on the substrate. The excess titanium in the film formed an Au−Ti alloy at high temperatures.[7,33] After many cycles of deposition and evaporation (TPD to 900 K) of $TiCl_x$ films, the XPS and AES analyses of the Au substrate found accumulation of a small amount of Ti in the substrate.

3c. Surface Structure of $TiCl_x$ Model Catalysts. The surface structure of the $TiCl_x$ multilayer film was characterized with thermal desorption behavior of a probe molecule. In previous studies,[9,13] mesitylene was found as a proper probe molecule because its desorption profile could differentiate a basal plane structure and a nonbasal plane structure of the $TiCl_x$ multilayer film. At low exposures (typically less than 1.4 L), mesitylene desorbs at ∼200 K from the basal plane sites and ∼250 K from the nonbasal plane sites. The basal plane has a closely packed structure of chlorine ions, having the lowest surface energy.[34] The nonbasal plane structure is not yet determined unambiguously, but it is clear that the nonbasal plane structure has a higher surface energy and lower chlorine density than the basal plane structure.

The mesitylene desorption profiles of the $TiCl_x$ multilayer films are shown in Figure 5. For the as-deposited film, the mesitylene desorption peaked at ∼220 K, which was higher than the desorption temperature from the basal plane (200K) but lower than that from the nonbasal plane (250 K). Knowing the almost complete coverage of chemisorbed $TiCl_4$ species (Figure 3), we tentatively assigned the 220 K peak to mesitylene adsorbed on the chemisorbed $TiCl_4$ species.

After removal of these chemisorbed $TiCl_4$ species by annealing at 580 K, the mesitylene TPD profile shifted to ∼250 K. This result indicated that the annealed film surface is composed of the nonbasal plane structure.

III-4. Postdeposition Electron Beam Irradiation of $TiCl_x$ Multilayer Films. The deposited $TiCl_x$ film could be reduced by irradiation of 500 eV electrons in the absence of the gas-phase $TiCl_4$. Table 2 describes significant reductions in the Ti oxidation state distribution upon irradiation of 4×10^{17} electrons/cm^2 at 300 K. Mostly, Ti^{4+} intensity decreased and Ti^{2+} intensity increased.

The reduction of Ti oxidation states upon electron irradiation was accompanied by changes in the TPD profiles of the irradiated film. Figure 6 compares the profiles of the $TiCl_y^+$($y = 1$, 2, 3, and 4) ions desorbing from the film before and after irradiation of 4×10^{17} electrons/cm^2 at 300 K. For the as-deposited film, the $TiCl_y^+$ profiles at <580 K followed the $TiCl_4$ fragmentation ratio in QMS. Above 580 K, the $TiCl_2^+$ profile had a slightly higher intensity than the $TiCl_3^+$ and $TiCl^+$ profiles. After electron irradiation, the $TiCl_4^+$ signal was not

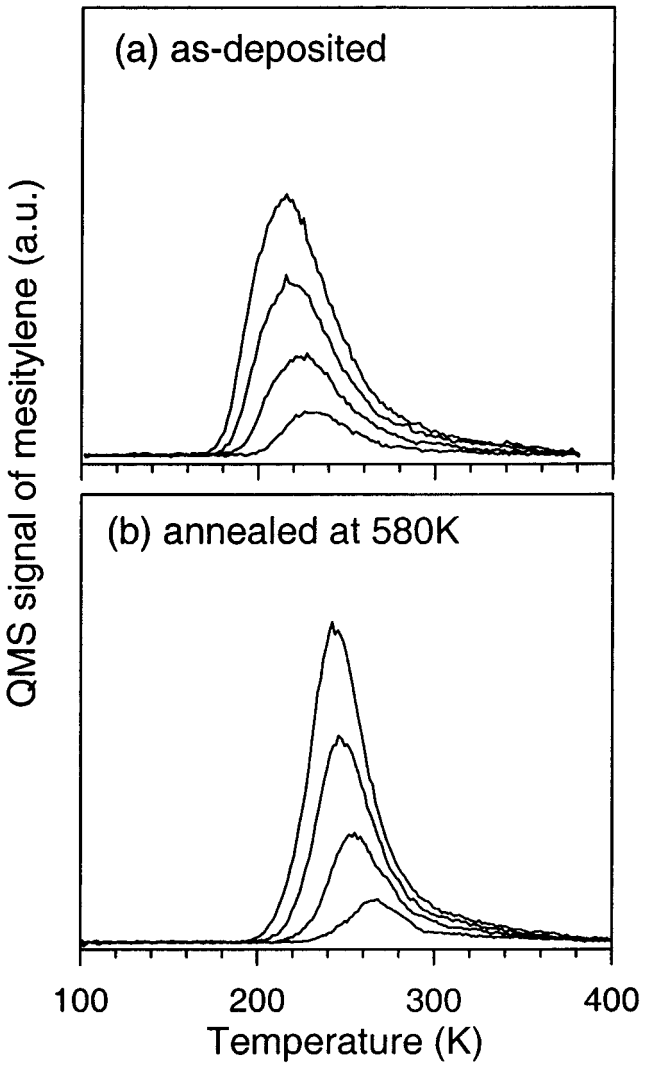

Figure 5. Mesitylene TPD of the $TiCl_x$ film (a) before and (b) annealing at 580 K. The mesitylene exposure was 0.2, 0.6, 1.0, 1.4 L, from the bottom. Deposition conditions: $P(TiCl_4) = 1 \times 10^{-7}$ Torr, electron energy = 500 eV, electron flux = 1.5×10^{14} electrons cm^{-2} s^{-1}, deposition time = 13 min.

TABLE 2: Effect of Post-Deposition Electron Irradiation on the Ti Oxidation State Distribution in $TiCl_x$ Film Deposited at 100 K (XPS measurement: 300 K)

	Ti oxidation state				
treatment	4+	3+	2+	1+	0
as-dosed[a]	76	21	1	2	0
e-irradiation[b]	52	7	34	7	0

[a] Deposition conditions: $P(TiCl_4) = 1 \times 10^{-7}$ Torr, electron energy = 500 eV, electron flux = 1×10^{14} electrons cm^{-2} s^{-1}, deposition time = 5 min. [b] Electron dose = 4×10^{17} electrons/cm^2 at 300 K.

detectable any more and the ions containing less chlorine atoms had a larger intensity ($TiCl^+ > TiCl_2^+ > TiCl_3^+$). This ion intensity distribution could be explained by desorption of $TiCl_3$(g), $TiCl_2$(g), or Ti_2Cl_6(g), but not $TiCl_4$(g), from the electron-irradiated film.

Previous studies with ISS and mesitylene TPD found that the electron irradiation of the deposited films caused desorption of chlorine ions from the film,[5,6,13] which was consistent with the reduction of Ti oxidation states in XPS and the increased intensities of chlorine-deficient ions in TPD. Some Ti ions could also desorb upon electron irradiation.[35] These effects caused a large error in film thickness estimation using AES.[7]

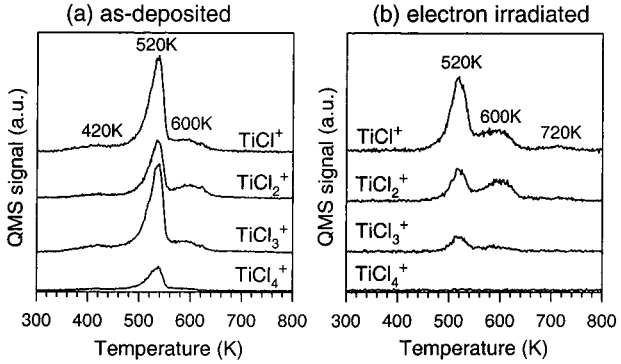

Figure 6. Effect of post-deposition electron irradiation on the desorption profiles of the $TiCl_y^+$ ($y = 1, 2, 3$, and 4) ions film measured with QMS during the TPD. Deposition conditions: $P(TiCl_4) = 1 \times 10^{-7}$ Torr, electron energy = 500 eV, electron flux = 1×10^{14} electrons cm^{-2} s^{-1}, deposition time = 5 min, and deposition temperature = 100 K. Post-deposition irradiation: electron energy = 500 eV; total electron dose = 4×10^{17} electrons cm^{-2}, film temperature = 300 K.

IV. Discussion

IV-1. $TiCl_x$ Film Deposition by Reactions between Electrons and Adsorbed $TiCl_4$. The $TiCl_x$ multilayer film, a model catalyst for stereospecific polymerization of propylene, was fabricated by electron-induced deposition of $TiCl_4$ on an inert gold substrate in UHV conditions. The deposition process could be modeled as processes in which the gas-phase $TiCl_4$ molecules impinge and physisorb on the surface at 100 K, the electron beam dissociates the adsorbed molecule into reactive species, and these species react to accumulate on the surface. In the absence of electrons, the adsorbed $TiCl_4$ molecules desorb intact from the surface.

The film deposition yield was first order in the electron flux (Figure 2a) and increased nonlinearly with the electron energy (Figure 2b). The primary electrons would ionize and fragment $TiCl_4$ molecules adsorbed at the surface:[36]

$$TiCl_4 + e^- (>20\ eV) \rightarrow TiCl_4^+ \quad (1)$$

$$\rightarrow TiCl_{(4-z)}^+ + zCl \quad (2)$$

The primary electrons of 500 eV would also generate secondary electrons of lower energy. The good fit between the deposition yield and Vaugan's form indicated the involvement of secondary electrons as well, most likely via dissociative electron attachment processes:[37]

$$TiCl_4 + e^- (3.8\ eV) \rightarrow TiCl_3^- + Cl \quad (3)$$

$$TiCl_4 + e^- (5.7\ eV) \rightarrow TiCl_3^* + Cl^- \quad (4)$$

These ionic and neutral species reacted with one another or with $TiCl_4$ and accumulated solid-phase $TiCl_x$ ($x < 4$) deposits on the substrate.

Under electron beam irradiation conditions, the deposited $TiCl_x$ could be reduced further. If this happened, the Ti oxidation state distribution and thermal evaporation behavior of the deposited film could change as the deposition time changes. However, this was not the case for the deposition at 100 K. This could be explained with the condensation of $TiCl_4$ at 100 K. The $TiCl_4$ molecules impinging on the surface would adsorb with nearly unit probability, forming a layer fluent with molecular $TiCl_4$ at the growing film surface. The impinging electrons of 500 eV would react predominantly with this

condensed $TiCl_4$ layer and only little could reach the $TiCl_x$ deposits underneath the $TiCl_4$ layer. In addition, the condensed layer could act as a barrier layer inhibiting desorption of dissociation fragments (such as chlorine atoms) into vacuum.[38] These effects would increase the chlorine concentration in the surface region of the film, giving rise to a higher oxidation state distribution of Ti.

IV-2. Stereospecific Polymerization of Propylene. The $TiCl_x$ multilayer film deposited under electron beam-irradiation conditions was stereospecific in Ziegler−Natta polymerization of propylene. After activation by reactions with $Al(C_2H_5)_3$, the $TiCl_x$ film produced exclusively isotactic polypropylene when it was exposed to 900 Torr of propylene gas. This result was obtained without any Lewis base added in the polymerization process.

The production of the stereospecific model catalyst lies in the electron beam irradiation during the catalyst deposition. In previous studies,[9,13,14] the $TiCl_x/MgCl_2$ films produced by thermal reactions of Mg and $TiCl_4$ on an Au substrate always had the basal plane structure at the surface and produced atactic polypropylene. In contrast, the $TiCl_x$ film produced by electron irradiation of $TiCl_4$ did not have basal plane structure but nonbasal plane structures exposed at the surface. Nonequilibrium conditions under electron beam irradiation appeared to cause the formation of energetically less favorable nonbasal plane structure. Electrons had hyper-thermal energy ranging from a few eV up to 500 eV in our experimental conditions. Reactions of these hyper-thermal electrons with $TiCl_4$ allowed a thermodynamically less favorable pathway forming the nonbasal plane structure with a high surface energy. Even if domains of the basal plane structure were formed at the film surface during the film deposition, a high flux of electrons would remove chlorine ions and convert the basal plane structure to the nonbasal plane structure.[13]

If the structure−stereospecificity relationship found from these model systems is pertinent to the high-surface-area Ziegler−Natta catalysts, the stereoselectivity enhancement effects of Lewis bases[1,2] could be rationalized by either blocking nonstereoselective polymerization sites on the basal planes or conversion of the basal plane surfaces to nonbasal plane structures. At present, it is not clear which is the case. The answer could be found in future studies investigating a correlation between electron beam or Lewis base treatments of a model catalyst containing the basal plane surface and the stereoselectivity of the treated model catalysts in propylene polymerization.

V. Conclusions

Electron beam-induced deposition of $TiCl_4$ on Au at 100 K produced a model Ziegler−Natta catalyst that was stereospecific in propylene polymerization. The deposition process was initiated by dissociation of $TiCl_4$ on the low-temperature substrate by electrons. The nonlinear increase of the deposition yield as a function of the electron energy at a constant current implied the involvement of low-energy secondary electrons in the deposition process. Reactions of dissociated fragments produced the solid-phase $TiCl_x$ deposits. The oxidation states of titanium near the film surface were mostly 4+, indicating a high concentration of chemisorbed $TiCl_4$ species. The deposited $TiCl_x$ film was stable at temperatures lower than 440 K. The film surface was composed of mostly nonbasal plane (defective) structures that selectively produced isotactic polypropylene. The absence of the most stable basal plane structure was due to the use of high-flux irradiation with electrons and low substrate temperature during the film deposition.

Acknowledgment. This work was supported by the Director, Office of Energy Research, Office of Basic Energy Sciences, Materials Science Division, of the U.S. Department of Energy under Contract No. DE-AC03-76SF00098. The authors also acknowledge support from Montell USA, Inc.

References and Notes

(1) Dusseault, J. J. A.; Hsu, C. C. *J. Macromol. Sci.- Rev. Macromol. Chem. Phys*. **1993**, *C33*, 103, and references therein.
(2) Barbè, P. C.; Cecchin, G.; Noristi, L. *Adv. Polym. Sci.* **1986**, *81*, 1.
(3) Gunter, P. L. J.; Niemantsverdriet, J. W.; Ribero, F. H.; Somorjai, G. A. *Catal. Rev—Sci. Eng.* **1997**, *39*, 77.
(4) Goodman, D. W.; Rainer, D. R *J. Mol. Catal. A* **1998**, *131*, 259.
(5) Magni, E.; Somorjai, G. A. *Surf. Sci.* **1995**, *341*, L1078.
(6) Magni, E.; Somorjai, G. A. *Surf. Sci.* **1996**, *345*, 1.
(7) Magni, E.; Somorjai, G. A. *J. Phys. Chem.* **1996**, *100*, 14786.
(8) Magni, E.; Somorjai, G. A. *J. Phys. Chem. B* **1998**, *102*, 8788.
(9) Kim, S. H.; Somorjai, G. A. *Appl. Surf. Sci.* **2000**, *161*, 333.
(10) Kim, S. H.; Somorjai, G. A. *J. Phys. Chem. B* **2000**, *104*, 5519.
(11) Kim, S. H.; Vurens, G.; Somorjai, G. A. *J. Catal.* **2000**, *193*, 171.
(12) Kim, S. H.; Somorjai, G. A. *Catal. Lett.* **2000**, *66*, 5.
(13) Kim, S. H.; Tewell, C. R.; Somorjai, G. A. *Langmuir* **2001**, *16*, 9414.
(14) Kim, S. H.; Somorjai, G. A. *J. Phys. Chem. B* **2001**, *105*, 3922.
(15) Mousty-Desbuquoit, C.; Riga, J.; Verbist, J. J. *Inorg. Chem*. **1987**, *26*, 1212.
(16) Hayashi, T.; Inoue, Y.; Chujo, R.; Doi, Y. *Polymer* **1989**, *30*, 1714.
(17) Busico, V.; Coradini, P.; De Martino, L.; Graziano, F.; Iadicicco, A. *Makromol. Chem*. **1991**, *192*, 49.
(18) Paukkeri, R.; Vaananen, T.; Lehtinen, A. *Polymer* **1993**, *34*, 4075.
(19) Gross, T.; Lippitz, A.; Unger, W. E. S.; Friedrich, J.; Woll, C. *Polymer* **1994**, *35*, 5901.
(20) Delhalle, J.; Riga, J.; Denis, J. P.; Deleuze, M.; Dosiere, M. *Chem. Phys. Lett.* **1993**, *210*, 21.
(21) Vaughan, J. R. M. *IEEE Trans. Electron Devices*, **1989**, *36*, 1963.
(22) Shih, A.; Hor, C. *IEEE Trans. Electron Devices*, **1993**, *40*, 824.
(23) Tong, W. H.; Williams, R. S. *Annu. Rev. Phys. Chem*. **1994**, *45*, 401.
(24) Kim, S. H.; Stair, P. C.; Weitz, E. *Chem. Phys. Lett.* **1999**, *302*, 511.
(25) Brand, V. P.; Sakmann, H. *Z. Anorg. Allg. Chem*. **1963**, *321*, 262.
(26) Kubaschewski, O. In *Titanium: Physicochemical properties of its compounds and alloys*; Komarek, K. L. Ed.; Atomic Energy Review Special Iss. No. 9, International Atomic Energy Agency: Vienna, 1983; Chapter 1.
(27) Briggs, D.; Seah, M. P. *Practical Surface Analysis, Volume 1—Auger and X-ray Photoelectron Spectroscopy*, 2nd ed.; J. Wiley & Sons: Chichester, U.K., 1990.
(28) Somorjai, G. A. *Introduction to Surface Chemistry and Catalysis*; John Wiley and Sons: New York, 1994; p 383.
(29) Redhead, P. A. *Vacuum* **1962**, *12*, 203.
(30) Nikitin, M. I.; Snigireva, E. M.; Tsirel′nikov, V. I. *Teplofiz. Vys. Temp*. **1993**, *30*, 1069.
(31) Sanderson, B. S.; Macwood, G. E. *J. Phys. Chem*. **1956**, *60*, 316
(32) Farber, M.; Darnell, A. J. *J. Phys. Chem*. **1955**, *59*, 156.
(33) Vilijoen, P. E.; Roux, J. P. *Vacuum* **1990**, *41*, 1746.
(34) Lin, J. S.; Catlow, C. R. A. *J. Mater. Chem*. **1993**, *3*, 1217.
(35) Tokutaka, H.; Prutton, M.; Higginbotham, I. G.; Gallon, T. E. *Surf. Sci.* **1970**, *21*, 233.
(36) Kiser, R. W,; Dillard, J. G.; Dugger, D. L. *Adv. Chem. Ser*. **1968**, *72*, 153.
(37) Bennett, S. L.; Pabst, R. E.; Margrave, J. L.; Franklin, J. L. *Int. J. Mass Spectrom. Ion Phys.* **1974**, *15*, 451.
(38) Kim, S. H.; Stair, P. C.; Weitz, E. *Langmuir* **1998**, *14*, 4156.